Evaluation of the inhibitory potential of Bioactive compounds against SARS-CoV2 by in-silico approach

Mariya Sneha Rani J
Kalasalingam Academy of Research and Education
Akkarshana P
Kalasalingam Academy of Research and Education
Neelaveni V
Kalasalingam Academy of Research and Education
Shalini Mohan
Kalasalingam Academy of Research and Education
Rajas M Rao
Yenepoya (Deemed to be University
Rekha PD
Yenepoya (Deemed to be University
Lakshmanan Muthulakshmi (l.muthulakshmi@klu.ac.in)
Kalasalingam Academy of Research and Education

Research Article

Keywords: SARS-CoV2, molecular docking, phytocompounds, anti-viral compounds, inhibitors, SwissADME, Lipinski's rule of five, Molecular dynamic simulation

Posted Date: September 28th, 2023

DOI: https://doi.org/10.21203/rs.3.rs-3371667/v1

Additional Declarations: No competing interests reported.

Version of Record: A version of this preprint was published at Journal of Molecular Modeling on February 7th, 2024. See the published version at https://doi.org/10.1007/s00894-024-05858-8.

Abstract

The COVID-19 (Coronavirus Disease 19) pandemic brought on by the SARS-CoV2 outbreak (Severe Acute Respiratory Syndrome Coronavirus 2) has stimulated the exploration of various available chemical compounds that could be used to treat the infection. This has driven numerous researchers to investigate the antiviral potential of several bioactive compounds from medicinal plants due to their reduced adverse effects compared to chemicals. Some of the bioactive compounds used in folklore treatment strategies are reported as effective inhibitors against the proliferative and infective cycles of SARS-CoV2. The secondary metabolites from plants are generally used to treat various diseases due to their intact medicinal properties. The present study analyses the inhibitory potential of phytocompounds from medicinal plants like Sphaeranthus indicus, Lantana camara and Nelumbo nucifera against SARS-CoV2 by molecular docking. Ten druggable protein targets from SARS-CoV2 are docked against the phytocompounds from the selected medicinal plants. The phytocompounds Astragalin, Isoquercetin, and 5-hydroxy-7-methoxy-6-c-glycosy flavone were found to have lower binding energy depicting their inhibitive potential compared with the reported inhibitors that are used in the treatment of SARS-CoV2 infection. To assess the compounds' potential as drugs, their ADMET characteristics were also examined. Sphaeranthus indicus, Lantana camara, Nelumbo nucifera six possible compounds were separately screened for ADME and toxicity characteristics, then the results were analyzed. Microsecond-level molecular dynamics simulations of both the ligands complexed with NSP15 revealed that the ligand induces allosteric effects on NSP15, which could lead to destabilization of NSP15 hexameric interface and loss of RNA binding.

Highlights

- Exploration of anti-viral properties of bioactive compounds from *Sphaeranthus indicus, Lantana camara and Nelumbo nucifera.*
- Phytocompounds with medicinal properties used in primordial treatment options are considered for the study.
- Molecular docking revealed compounds with the ability to inhibit the replication and breakage of polyprotein in the SARS-CoV2 virus.
- Molecular dynamic simulation of NSP15 with the ligand showed the binding of ligand might lead to loss of RNA binding.

Introduction

Medicinal plants are one of the valuable sources for discovery of therapeutic compounds that are potential inhibitors for several diseases and ailments. The evolution of virulent organisms and the multidrug resistance acquired by them has led to a surge in the exploration of a ginormous number of new molecules making phytocompounds a thriving option for drug discovery and development. The bioactive compounds draw significant attention due to their reduced side effects compared to modern allopathic treatments [1]. Herbal formulations like ‘Kabasura kudi neer’ and ‘Nilavembu kashayam’ are used as supplementary medicine for COVID-19 and Dengue fever respectively as recommended by the government to boost our immune system [2, 3].

Medicinal plants like *Lantana camera*, *Nelumbo nucifera*, and *Sphaeranthus indicus* that are traditionally used for treating various diseases have been selected for this study. *Lantana camera* is an Ayurvedic plant used by tribal people [1]. It is found in various parts of India like Tamil Nadu, Kerala, Karnataka, Maharashtra, and Manipur and has ethno-medicinal properties to treat many health problems. The important phytocompounds present in *L. camera* are beta caryophyllene, germacrene D, alpha humulene, and Terpineol [4, 5]. *Sphaeranthus indicus* is used in traditional Indian system of medicine for curing various ailments [6]. Some bioactive compounds of *S. indicus* such as 5*α*-hydroperoxy-7*α*-hydroxy-isosphaerantholide, (11*α*,13-dihydro-7*α*-hydroxyfrullanolide-13-yl)-adenine, 5*α*-hydroxy-isosphaerantholide, 11*α*,13-dihydro-eudesman-3,5,7-triene-6*α*-12-olide [7], alpha –hydroxyfrullanoide are reported to have anti-tumor activity [8]. *Nelumbo nucifera* (Thaaramai) is an aquatic plant species found in India, across wide geographic distributions spreading between Himalayas to Tamil Nadu [9]. It is used to treat sunstroke, diarrhoea, improve the skin condition, and urinary problems [10]. Flavonoids like kaempferol, trifolin, astragalin, kaempferol 3-O-gln, quercetin, isoquercetin, and rutin are the most important secondary metabolites of lotus [11].

SARS-CoV2 (Severe Acquired Respiratory Syndrome Coronavirus 2) is the viral pathogen responsible for the COVID-19 pandemic as declared by WHO on 17th of April 2020. The pathogen has affected almost all the countries around the globe and has symptoms that are more likely to normal flu infections. Yet this virus has high evolutionary rate with $8*10^{-4}$ substitutions per site, approximately with one mutation for every two weeks [12]. The infection produces a wide range of ailments from an asymptomatic transporter state to gentle and serious cold-like manifestations to a deadly pneumonia. The virus is built up of structural proteins like spike, nucleocapsid and envelope protein, and non-structural proteins 1–16 (NSP) with varying functions to regulate molecular machinery that help viral proliferation and infections [13]. Thereby, protein targets of SARS-CoV2 are docked against the phytocompounds from the selected plants using AutoDock Vina to evaluate their ability to act as potential inhibitors.

Computer-aided drug ADME (Absorption, Distribution, Metabolism, and Excretion) computation was taken into consideration to provide reliable and anticipatory data to the experiment. These computing models describe the therapeutic, physicochemical, and pharmacokinetic characteristics of micro-compounds. The Swiss Institute for Bioinformatics (SIB) promotes the use of bioinformatics resources by scientists around the world. One of their most current and extensive websites is the SwissADME [14]. It allows the evaluation of ADME parameters of drug candidates and compounds and provides data that aids in the assessment of antecedent uncertainty in the drug discovery process; it is the rostrum to establish Lipinski's rule of five. Drug likeness is an assessment of how exactly a molecule resembles a recognized drug in terms of its electron distribution, hydrophobicity, hydrogen bonding qualities, molecular flexibility, and size, among other attributes of molecules and structural features. According to Daina and Zoete (2016) [15], one of the additional features of SwissADME is the BOILED-Egg assessment, which predicts gastrointestinal absorption (HIA) and efflux/retention using P-glycoprotein. The purpose of the current study was to submit the bioactive substances found in *Sphaeranthus indicus, Lantana camara, Nelumbo nucifera* for *in silico* ADMET screening utilizing the SwissADME website (http://www.swissadme.ch/index.php) in order to assess each compound's unique ADME behaviour, including its physiochemical characteristics, Lipophilicity, water solubility, pharmacokinetics, drug-likeness, and medicinal chemistry qualities. The top-ranked ligands' druggability and toxicity risks were predicted based on their characteristics for absorption, distribution, metabolism, excretion,

and toxicity (ADMET). The results were interpreted and further data augmented. Thereby, protein targets of SARS-CoV2 were docked against the phytocompounds from the selected plants using AutoDock Vina to evaluate their ability to act as potential inhibitors and the ADME properties were predicted. Molecular dynamics simulation of the top binder ligand and the target protein was performed using GROMACS program and the local level effects, global level effects and the allosteric effect of the ligand binding with the NSP 15 protein analysed.

Materials and Methods

Protein target and ligand collection

The structures of the protein targets from the SARS-CoV2 virus namely NSP 3, NSP 5, NSPP 7, NSP 8, NSP 12 [16], NSP 9 [17], NSP 13 [18], NSP 14 [19], NSP 15 [20], and Spike protein [21] as shown in Table 1, were retrieved from Protein Data Bank (PDB) [22]. The 3D structures of the selected ligands were retrieved from PubChem chemical compound database as shown in Fig. 1.

Table 1
Functions of the chosen protein targets from SARS-CoV2 and their PDB ID.

S. No.	Protein target	Function	PDB ID	Reference
1.	NSP 9	Replicase	6W9Q	[17]
2.	NSP 10	mRNA capping, Cofactor of NSP 16, NSP 14	6W61 (Chain B)	[23]
3.	NSP 12	RNA dependent RNA polymerase	6M71	[16]
4.	NSP 13	Helicase	6JYT (Chain A)	[21]
5.	NSP 14	Proofreading exoribonuclease	5NFY (chain A)	[19]
6.	NSP 15	Endoribonuclease	6VWW	[20]
7.	NSP 16	Methytransferase, mRNA capping	6W61 (Chain A)	[23]
8.	Mpro (NSP 5)	Main protease	6LU7 (Chain A)	[24]
9.	Plpro (NSP 3)	Papain like protease	7JRN (Chain A)	[25]
10.	Spike protein	Aids binding to receptors	2AJF (Chain A)	[21]

Molecular docking

The target protein and the study ligands were prepared for the study by initial removal of water molecules and heteroatoms using Discovery Studio Visualizer. Then hydrogen atoms and Kollman charges were added to it using Auto Dock tools [26]. The protein and ligands were then converted to ‘pdbqt’ file format that contained the information about atomic charges, number of rotatable bonds using Auto Dock Tools package [27]. Molecular Docking was then performed for the prepared ligand using Auto Dock tools [28]. The binding energy and the amino acids of the protein responsible for the interaction were visualized using Discovery Studio Visualizer [29].

Drug-likeness and toxicity predictions

The drug-likeness was predicted using Lipinski's rule of five, which establishes the consistency of an oral active medication. The Lipinski's rule makes predictions about a compound's permeability or absorption. Lipinski's requirements state that three of the following values should be met: a molecular weight of 500 Daltons (Da), a calculated lipophilicity of 5 (Log P), a number of hydrogen-bond acceptors and donors of 10 and 5 respectively, and a calculated lipophilicity of 5. Higher drug score values indicate that a compound may be a potential drug candidate [30]. OSIRIS Property Explorer and the Swiss ADME predictor were used in this study to screen the compounds. Using the SWISS ADME (http://www.swissadme.ch) tool, Lipinski parameters were predicted [31]. The data on the amount of hydrogen acceptors, hydrogen donors, and rotatable bonds was provided by the Swiss ADME predictor. Using the OSIRIS Property Explorer software, the analyzed compounds were screened, and only those that did not break Lipinski's rule were utilized to assess the mutagenic, reproductive hazards, irritating and tumorigenic, hydrophilicity, molecular weight, solubility, drug-likeness, and drug score. Using the same software, solubility (Log S) was also predicted; Log S-4 denoted good solubility and favorable compound absorption [32].

ADMET prediction

The pharmacokinetic features of the ligands-absorption, distribution, metabolism, excretion, and toxicity-must be assessed in order to ascertain their activity in the body. AdmetSAR, is an online prediction tool for ADMET properties, was used to examine the ligands properties (http://lmmd.ecust.edu.cn/admetsar2/).The boiled egg allows for the evaluation of brain penetration (BBB) and passive gastrointestinal absorption (HIA); the white portion of the egg indicates a high possibility of passive absorption through the gastrointestinal tract, and the yolk indicates a high probability of brain penetration. Additionally, the dots are marked red if they are anticipated to not be a P-gp substrate and blue if they are predicted to be actively effluxed by P-gp (PGP+) [33].

Molecular simulation:

Ligand parameterization:

The ligands with maximum binding affinity to NSP15 from the docking studies (5-Hydroxy-7-methoxy-6-c-glycosyflavone or 5-HF and Isoquercetin or ISQ) were simulated in complex with NSP15. Parameters for both the ligands were generated using Antechamber program [34]. Atom charges were assigned using AM1-BCC model [55]. The ligand parameters were converted to GROMACS compatible formats using ACPYPE program [35]. To ensure that parameters are consistent with molecular properties observed from experiments, energies associated with dihedral angles of 5-HF were compared the energies identified from previous DFT studies [36]. Comparison was performed by generation of different torsional conformations of -OH group of 5-HF using UCSF Chimera program [37]. On the generated conformations, energies associated with each dihedral angle was calculated by performing energy minimization in vacuum for single step using GROMACS program [38, 39]. The net potential energy of the system associated with each dihedral angle were plotted and compared with the quantum chemistry studies previously performed on 5-HF. The generated parameters above were also used for the molecular dynamic simulations of both the ligands in complex with NSP15.

Molecular dynamics simulations:

All the preparation and production are performed using GROMACS 2020.4 program [38, 39]. Top-scoring complexes of 5-HF and ISQ with NSP15 (with binding energies of -9.3kcal/mol and − 8.2kcal/mol respectively as observed from the docking studies) were used as the initial structures for the simulations. The cryo-electron microscopic structure of SARS-CoV2 NSP15 protein (PDB:7K0R) was used as the starting structure for the simulations [20]. The protein was described using AMBER99SB-ILDN force field [40], the ligands were described using the parameters generated as described above. The system was solvated in a cubic box with an edge distance of 2.0nm; water was described using TIP3P model [41, 42, 43, 44]. The production simulations were performed initially for 100 ns and later extended to 250 ns, with timestep of 2 fs. Three more such replicates were simulated for 250 ns each, resulting in a total sampling of 1μs.

Analysis of simulation trajectories:

For analysis of the simulation trajectories, processing of all the trajectories was performed using gmxtrjconv tool of GROMACS. The trajectories of all the replicates were concatenated into a trajectory ensemble. Analyses were performed on three trajectory ensembles, corresponding to simulations of NSP15 in complex with 5-HF, ISQ and NSP15 without any bound ligands. All the following analyses were performed on these trajectory ensembles. To assess the longevity of ligand binding with the NSP15, minimum distance of ligand with the protein was calculated using gmxmindist tool of GROMACS [38, 39]. Calculations were performed on all the backbone as well as side chain atoms of NSP15. The fluctuations were represented on the NSP15 structure as b-factors, and visualized using UCSF Chimera program [37]. The NSP15 structure with residue fluctuations represented as b-factors was superimposed over the cryo-electron microscopic structure of SARS-CoV2 endoribonuclease [45] (NSP15; PDB: 7TJ2). Dynamics of hexamer interface residues as well as RNA-binding interface was characterized based on the superimposition with respect to the cryo-electron microscopic structure. The global-level effects of ligand binding on NSP15 dynamics were performed by Principal Component Analysis (PCA) was performed using ProDy program. The essential dynamics associated with the first eigenvectors of the three trajectory ensembles (NSP15 + 5-HF, NSP15 + ISQ & NSP15 without ligand) were extracted and visualised using the normal mode wizard of the VMD program [54]. The allosteric effects associated with the ligand binding to NSP15 were studied using the perturbation residue scanning calculations, using ProDy program [46]. Effectiveness (tendency of residue to induce allosteric dynamics) and Sensitivity (tendency of a residue to undergo allosteric dynamics) profiles was calculated, and projected over the NSP15 structure. The sensitivity and effectiveness profiles were visualised using the UCSF Chimera program [37].

Results and Discussion

Upon performing molecular docking of the protein targets of SARS-CoV2 and the phytocompounds of *Lantana camera, Sphaeranthus indicus*, and *Nelumbo nucifera* the binding energies (in kcal/mol) were identified and compared with the available inhibitors used for the treatment of SARS-CoV2 infection (Table 2).

Table 2
Binding energies of phytocompounds and reported inhibitors against protein targets of SARS-CoV2

Protein targets	Reported inhibitors	Binding energy (kcal/mol)					
		Nelumbo nucifera		Sphaeranthus indicus		Lantana camara	
		Astragalin	Isoquercetin	7-Hydroxy frullanolide	5-hydroxy-7-methoxy-6-c-glycosy flavone	Germacrene D	Terpinol
NSP 7		-5.8	-6	-5.9	-6.2	-5.4	-4.8
	Suramin	-9.2					
NSP 8		-5.7	-5.3	-5.4	-6.2	-3.9	-4.9
	Suramin	-8.6					
NSP 9		-6.4	-6.8	-6.5	-7.3	-5.8	-5
	Conivaptan	-10.2					
NSP 12		-7.9	-8.2	-6.7	-7.9	-5.6	-5.1
	Remdesivir	-7.7					
NSP 13		-8.3	-7.5	-8.2	-7.4	-6.8	-5.3
	Suramin	-12.5					
NSP 14		-8.1	-8	-6.7	-7.9	-7.3	-6.4
	Putulin	-4.9					
NSP 15		-8.2	-8.3	-7.9	-9.3	-5.7	-6.3
	NSC 95397	-6.7					
Mpro (NSP 5)		-7.5	-8.2	-6.6	-7.8	-5.7	-5.3
	GTPL10716	-6.9					
Plpro (NSP 3)		-6.9	-7	-7.2	-6.8	-5.3	-6.4
	GRL0617	-9.3					
Spike		-7.4	-7.8	-7.2	-7.6	-6	-5.6
	Tegobuvir	-9.3					

From the docking results, it could be interpreted that the candidate phytocompounds were better binders for the target proteins NSP12, NSP14, NSP15 and Mpro. The ligands of *Sphaeranthus indicus* and *Nelumbo*

nucifera were effective binders of the targets NSP12, NSP14, NSP15 and Mpro whereas the ligands of *Lantana camera* were effective binder of the target NSP14. The 2D and 3D interactions of the top binders were shown in Fig. 2a-2d for interactions between NSP12 and Isoquercetin, NSP14 and Astragalin, NSP15 and 5-hydroxy-7-methoxy – 6-c-glycosy flavone and NSP5 and Isoquercetin respectively. Hence, the chosen phytocompounds were proposed to possess anti-viral property against the target proteins of SARS-CoV2 that are responsible for the replication and protein lysis mechanisms.

Drug-likeness and ADMET property prediction

Supplementary Table 1 showed the physiochemical parameters of the ligands predicted using Swiss ADME. After screening and filtration using Lipinski's rules, 6 potential active compounds were retained. Generally, Lipinski's rule states that an orally active drug can have no more than one violation of the Lipinski's rule parameters [47]. Based on the polarity of the molecules, the permeation method known as BOILED-Egg (Brain or Intestinal EstimateD) calculates the lipophilicity with more accuracy. The drug-likeliness property, the number of violations of Lipinski's rule, and the BOILED-Egg plot are calculated using the canonical SMILES notation of the binders as input through the OSIRIS property explorer tool and ADME server, respectively.

OSIRIS Property Explorer was used to identify the drug-likeness characteristics of cLogP, LogS, Molecular Weight, TPSA, and drug score compounds. Higher hydrophilicity of the substances, as determined by this technique, indicated better absorption and penetration. Low log S values signified increased solubility, which might increase absorption. Additionally, a low molecular weight can increase the rate of absorption. Topological Polar Surface Area (TPSA) is a property of the compound's polar atoms, and a lower TPSA was preferable for drug-like properties. Additionally, this tool predicted reproductive toxicity, irritability, mutagenicity, and tumorigenicity [31, 33].

The BOILED-egg plots depicted in Supplementary Fig. 1 that all the top binders were capable of absorption into the human gastrointestinal tracts. 5-hydroxy-7-methoxy-6-C-glycosylflavone is predicted to possess some resistance against the drug efflux mediated by P-glycoprotein because of their lower value of TPSA.

Supplementary Table 2 showed the notable ADMET properties of the phytocompounds chosen for the study. It was found that the top binders from molecular docking were biodegradable and not toxic to the respiratory and reproductive systems. Table 3 listed some of the medicinal properties of the phytocompounds.

Table 3
Medicinal properties of the phytocompounds.

Top binder	Botanical name of the medicinal plant	Medicinal properties of plant	Reference
7-Hydroxyfrullanolide	*Sphaeranthus indicus*	Inhibits colorectal cancer cell growth	[48]
5-hydroxy-7-methoxy-6-C-glycosylflavone	*Sphaeranthus indicus*	Appetizer, digestant, laxative vermicide and liver stimulant, hence, beneficial in anorexia, dyspepsia, constipation, worm infestations, piles, splenomegaly and hepatitis, extremely useful in epilepsy, mental debility and as a nervine tonic.	[49]
Terpineol	*Lantana camara*	Treatment of tumors, tetanus, rheumatism and malaria.	[50]
Germacrene D	*Lantana camara*	The stem, root and leaves contain many of the bioactive compounds responsible for various therapeutic applications such as cancers, chicken pox, measles, asthma, ulcers, swellings, eczema, tumors, high blood pressure, bilious fevers, catarrhal infections, tetanus, rheumatism, malaria, antiseptic, antispasmodic, carminative and diaphoretic.	[51]
Astragalin	*Nelumbo nucifera*	It is used to treat sunstroke, diarrhea, dysentery, hemorrhoids, dizziness, vomiting of blood, uterine bleeding disorders, promoting conception, improving the skin condition, controlling burning sensation, against infections, cough, hypertension, fever, urinary problems, hematemesis, epistaxis, hemoptysis, hematuria, and metrorrhagia etc	[10]
Isoquercetin	*Nelumbo nucifera*	The whole plant is used as an herbal medicine to cure diarrhea, insomnia, fever, body heat imbalance, gastritis and release skin inflammatory symptoms.	[52]

Molecular simulation

Protein-ligand contact patterns in the simulations:

To understand if the protein-ligand contacts observed in the docking are preserved in the simulations, the contact frequencies between the NSP15 residues and both the ligands (5-HF and ISQ) were calculated. For the 5-HF, many of the protein-ligand contacts observed in the docking experiments are largely conserved in the simulations (SF2A). However, for ISQ, though many of the protein-ligand contacts obserced in the docking were also observed in the simulations, the most frequent contacts were not the ones observed in the docking. The residues with highest frequency of contacts with ISQ were the residues 200–202, and the residues 267, 278 & 280. These residues are not observed as contacts in the docking experiments. Emergence of these residues as contacts in the simulations suggests that there is a shift in the protein-ligand contacts. Despite this, the overall binding cavity of both 5-HF and ISQ remains conserved in the MD simulations. It is also worth noting that both the ligands bind to the similar region of NSP15, which led us to hypothesize that both the ligands could elicit similar effects on the NSP15 structure and dynamics.

Local-level effects of ligand binding on NSP15 dynamics: SARS-CoV2 NSP15 consists of three domains: N-terminal oligomerization domain, Middle domain and NendoU ribonuclease domain (Fig. 5A). The N-terminal oligomerization domain is critical for functional activation of NSP15, which involves oligomerization of NSP15 molecules (Deng & Baker 2018). Middle domain is involved in the RNA binding (Deng & Baker 2018, Kim et al. 2020), and the NendoU domain has the ribonuclease activity (Kim et al. 2020). To understand how the impact of ligand binding affects the local fluctuations of NSP15 residues, RMSF calculations were performed. The fluctuations were represented as B-factors and projected on the NSP15 structure. NSP15 in absence of ligand is largely rigid. Most of the residues in absence of a ligand have mean fluctuations between 1–2Å (Fig. 5B, E). The only dynamic residues in the apo-state of NSP15 are the residues that from a beta hairpin between residues 35 to 42, particularly the residue D37 (Fig. 5B, E). In contrast, in presence of both the ligands, numerous NSP15 residues are destabilized. In the simulations of 5-HF bound to NSP15, many of the NSP15 residues are found to have higher fluctuations (Fig. 5C). However, the Oligomerization domain particularly is destabilized in 5-HF bound NSP15. While the fluctuations of the oligomerization domain are on an average 2Å in the apo-state, the fluctuations in the 5-HF bound state vary between 4.5-8Å (Fig. 5B). Additionally, RNA-binding residues K112 and T114 are also destabilized in the 5-HF bound state, with the mean fluctuations between 6.5-7Å. ISQ also elicited similar effects, where the N-terminal oligomerization domain was found to be destabilized. In fact, ISQ induced greater amount of destabilization compared to 5-HF, as the residues of oligomerization domain were found to have 0.5-1Å more fluctuations when ISQ was bound to NSP15 (Fig. 5B).

Superimposition of the NSP15 showing fluctuations as B-factors over the hexameric cryo-electron microscopic structure of NSP15 revealed the potential impact of ligand binding on the stability of the NSP15 hexameric interface. Since the β-hairpin formed by the residues 30–50 forms a protrusion that enables oligomerization with other monomers, destabilization of this region suggests that NSP15 oligomerization may be significantly affected in the ligand bound states. Similar observations are also made for the ISQ-bound NSP15 (Fig. 5C,D). In both the ligand-bound states, the protrusion formed by the β-hairpin that constitutes N-terminal oligomerization domain is destabilized, suggesting that NSP15 oligomerization may be perturbed upon binding by both the ligands. In contrast, such destabilization of β-hairpin is not observed from the apo-state simulations, it may be inferred that this region is otherwise rigid, and contributes to the stability of the hexameric interface (Fig. 5E). Given the fact that oligomerization of NSP15 into a hexameric unit is critical for its functioning, disruption of its oligomerization could ultimately result in disruption of its function.

Global-level effects of ligand binding on NSP15 dynamics

To understand how dynamics of each of the domains & the global NSP15 dynamics are affected by the ligand binding, we performed principal component analysis on the C-alpha atoms of NSP15 trajectory ensembles. Dynamics associated with the first eigenvector was visualised. When the first eigenvector dynamics of NSP15 bound to 5-HF, ISQ & unbound states were compared, it is clear that there are large-scale changes in the global NSP15 dynamics. In the 5-HF-bound NSP15 trajectory, the oligomerization domain underwent bending dynamics, where the domain bent towards the NendoU domain (Fig. 6A). Simultaneously, the middle domain, particularly the RNA-binding helix stretched outwards (Fig. 6A). On the other hand, in the ISQ bound NSP15, the oligomerization domain stretched so that the distance between the secondary structural elements among the oligomerization increased (Fig. 6B). Similarly, NendoU domain in the ISQ

bound NSP15 bent away from the other 2 domains. Compared to both the ligand-bound trajectories, NSP15 in the absence of ligand exhibited different dynamics, were both the oligomerization domain and NendoU domain converged towards each other (Fig. 6C). While distinct global-level dynamics are observed on NSP15, the magnitude of such dynamics are much higher in the ligand-bound trajectories, as seen from the length of the porcupine arrows (Fig. 6).

From the analysis of essential dynamics of NSP15 from PCA, we infer that the observations at the local level made from RMSF calculation also translate to the global level, where global NSP15 dynamics in ligand-bound states could result in NSP15 destabilization. For instance, the destabilization of the oligomerization interface may accompany stretching of the oligomerization domains in ISQ bound state (Fig. 6B). Similarly, the perturbation of NSP15-RNA interactions could arise from the large-scale dynamics of the RNA-binding residues observed in the 5-HF bound state (Fig. 6A).

Allosteric effects of ligand binding on NSP15

Since the large-scale changes in NSP15 dynamics are localized at regions that are located at long distances from the ligand binding pocket (> 8–10Å), we hypothesized that the dynamics induced by the ligand binding could be allosteric. To evaluate whether the dynamics of the oligomerization domain induced by ligand binding are allosteric in nature, perturbation residue scanning calculations were performed. Perturbation Residue Scanning calculations were performed according to the methodology developed by Dutta et al., (Dutta et al. 2015) where impact of dynamics of allosteric residue from perturbation of binding residue is calculated from the dynamics of the calculated eigenvectors from principal component analysis. Based on the residue perturbations, sensitivity (propensity of residues to act as sensors of allosteric dynamics) as well as effectivity (propensity of residues to trigger allosteric dynamics) profiles were calculated and projected over the structure of NSP15. In the presence of both the ligands, we found that the residues of the N-terminal oligomerization domain, particularly the residues forming the β-hairpin (residues 37–42) as well as other residues of the oligomerization domain (residues N30, 48–51 in ISQ bound NSP15) are found to be the residues with the highest sensitivity (Fig. 7A, C). On the other hand, the residues that form the binding pocket (residues 251 to 255 & residue D298) are found to be the strongest effectors, in the presence of both ligands (Fig. 4B, D). Interestingly, most of the effectors are aliphatic residues, comprising of isoleucine, leucine, and glycine (with the exception of D298 and H251, bound to ligands 5-HF and ISQ respectively). These residues could primarily interact with the aromatic rings of both the ligands, triggering the allosteric dynamics of oligomerization domain. Thus, it is clear that both the ligands destabilize NSP15 through an allosteric mechanism, in which upon binding, the residues of the oligomerization domain are destabilized, resulting in the destabilization of the NSP15 hexameric interface and disruption of the NSP15-RNA binding. As a result of this, loss of hexameric interface could perturb NSP15 function, ultimately negating the immunosuppressive effects of NSP15.

Conclusions and perspective

The low binding energy exhibited by the phytocompounds from *Lantana camera, Sphaeranthus indicus*, and *Nelumbo nucifera* against the protein targets of SARS-CoV2 showed inhibitory potential by the selected molecules. Their predicted interference of the enzymes involved in the molecular mechanisms aiding the proliferation of SARS-CoV2 indicated the inhibitive ability of the phytocompounds.

In the present study, SwissADME, ADMETSAR web tools were used to evaluate hit molecules present in *Sphaeranthus indicus, Nelumbo nucifera, Lantana camara*. From this study, the ADME property of the phytocompounds was disclosed and it can be used as appropriate tool for further identification of their *in vitro* therapeutic potentials.

In recent past, there has been a lot of interest concerning medicinal plants. Particularly, much of this interest is focussed on the secondary metabolites in the plants and their potential in treatment of various pathological conditions (Gorlenko et al. 2020). In this study, we have demonstrated the therapeutic role of such metabolites against the SARS-CoV2 infection. We found from the docking studies that two such metabolites, 5-Hydroxy-7-methoxy-6-c-glycosyflavone and Isoquercetin bound to the NSP15 protein of SARS-CoV2 with high affinity. Microsecond-level molecular dynamics simulations of both the ligands complexed with NSP15 revealed that the ligand induces allosteric effects on NSP15, which could lead to destabilization of NSP15 hexameric interface and loss of RNA binding. Such effects could ultimately result in the loss of immunosupressive effects of NSP15, paving way for immune response from the host.

Declarations

Acknowledgements:

The authors thank the Kalasalingam Academy of Research and Education, Srivilliputhur, India for providing with the facilities throughout this work. The authors also thank the financial resources and infrastructural support from Yenepoya (Deemed to be University). The authors also thank the ROMEO-HPC of Université de Reims Champagne-Ardenne, France for computational resources for the MD simulations.

Ethical Approval:

Not applicable

Funding:

Ms. Shalini Mohan, Junior Research Fellow acknowledges the Department of Biotechnology (DBT), Government of India for the financial grant offered with the fellowship ID DBT/2022-23/KARE/2059. Dr. Lakshmanan Muthulakshmi acknowledges the Department of Scientific and Industrial Research for the financial grant (DSIR/TDUPW-1101/3/2021-IRD (SC)/-DSIR and Kalasalingam Academy of Research and Education for seed money grant in the year 2021-2022.

Conflict of interests:

The authors declare that they have no known competing financial interests or personal relationships that could have appeared to influence the work reported in this paper.

Data availability statement:

The authors confirm that the data supporting the findings of the study are available within the article.

Author contributions:

RMR and RPD designed the simulation experiments. RMR performed the molecular dynamics simulations and analysis. RPD contributed to the analysis of simulations. All the authors wrote the manuscript, revised and gave approval for the final version of the manuscript.

References

1. Ignacimuthu, S., Ayyanar, M., &Sankarasivaraman, K. (2008). Ethnobotanical study of medicinal plants used by Paliyar tribals in Theni district of Tamil Nadu, India. *Fitoterapia*, 79(7–8), 562-568.10.1016/j.fitote.2008.06.003
2. Kiran, G., Karthik, L., Devi, M. S., Sathiyarajeswaran, P., Kanakavalli, K., Kumar, K. M., & Kumar, D. R. (2020). In silico computational screening of KabasuraKudineer-official Siddha formulation and JACOM against SARS-CoV-2 spike protein. *Journal of Ayurveda and Integrative Medicine*, 100324.10.1016/j.jaim.2020.05.009
3. Ramalingam, V., &Venkataramani, G. (2020). Unlocking the Potential of Traditional Native Medicines-A Perspective to Manage the COVID-19 Pandemic. Journal of Research in Traditional Medicine, 6(1), 21–8.
4. Khan, M., Srivastava, S. K., Syamasundar, K. V., Singh, M., & Naqvi, A. A. (2002). Chemical composition of leaf and flower essential oil of Lantana camara from India. *Flavour and Fragrance Journal*, 17(1), 75-77.10.1002/ffj.1047
5. Nea, F., Tanoh, E. A., Yapi, T. A., Garcia, G., Tomi, F., & Tonzibo, Z. F. (2017). Chemical investigation on leaf, flower and fruit oils of lantana camara from Côte d'Ivoire. Natural Product Communications, 12(4), 1934578X1701200434.
6. Ramachandran, S. (2013). Review on Sphaeranthus indicus Linn. (Koṭṭaikkarantai). Pharmacognosy Reviews, 7(14), 157. 10.4103/0973-7847.120517
7. Mahajan, N. G., Chopda, M. Z., & Mahajan, R. T. (2015). A review on Sphaeranthus indicus Linn: Multipotential medicinal plant. International Journal of Pharmaceutical Research and Allied Sciences, 4(3), 48–74.
8. Emani, L. R., Ravada, S. R., Garaga, M. R., Meka, B., & Golakoti, T. (2017). Four new Sesquiterpenoids from Sphaeranthus indicus. *Natural Product Research*, 31(21), 2497-2504.10.1080/14786419.2017.1315576
9. Lin, Z., Zhang, C., Cao, D., Damaris, R. N., & Yang, P. (2019). The latest studies on lotus (Nelumbo nucifera)-an emerging horticultural model plant. *International Journal of Molecular Sciences*, 20(15), 3680.10.3390/ijms20153680
10. Sheikh, S. A. (2014). Ethno-medicinal uses and pharmacological activities of lotus (Nelumbo nucifera). Journal of Medicinal Plant Studies, 2(6), 42–46.
11. Chen, G., Zhu, M., & Guo, M. (2019). Research advances in traditional and modern use of Nelumbo nucifera: phytochemicals, health promoting activities and beyond. *Critical reviews in Food Science and Nutrition*, 59 (sup1), S189-S209.10.1080/10408398.2018.1553846
12. Domingo-Calap, P., Schubert, B., Joly, M., Solis, M., Untrau, M., Carapito, R., …Bahram, S. (2018). An unusually high substitution rate in transplant-associated BK polyomavirus in vivo is further concentrated in HLA-C-bound viral peptides. *PLoS pathogens*, 14(10), e1007368.10.1371/journal.ppat.1007368

13. Garcia-Beltran, W. F., Lam, E. C., Denis, K. S., Nitido, A. D., Garcia, Z. H., Hauser, B. M., Feldman, J., Pavlovic, M.N., Gregory, D.J., Poznansky, M.C. & Balazs, A. B. (2021). Multiple SARS-CoV-2 variants escape neutralization by vaccine-induced humoral immunity. Cell, *184*(9), 2372–2383. https://doi.org/10.1016/j.cell.2021.03.013
14. Ndombera, F., Maiyoh, G., & Tuei, V. (2019). Pharmacokinetic, physicochemical and medicinal properties of n-glycoside anti-cancer agent more potent than 2-deoxy-d-glucose in lung cancer cells.
15. Daina, A., & Zoete, V. (2016). A boiled-egg to predict gastrointestinal absorption and brain penetration of small molecules. *ChemMedChem*, 11(11), 1117-1121.10.1002/cmdc.201600182
16. Kirchdoerfer, R. N., & Ward, A. B. (2019). Structure of the SARS-CoV nsp12 polymerase bound to nsp7 and nsp8 co-factors. *Nature Communications*, 10(1), 1-9.10.1038/s41467-019-10280-3
17. El-Kamand, S., Du Plessis, M. D., Breen, N., Johnson, L., Beard, S., Kwan, A. H., Richard, D.J., Cubeddu, L. & Gamsjaeger, R. (2022). A distinct ssDNA/RNA binding interface in the Nsp9 protein from SARS-CoV-2. *Proteins: Structure, Function, and Bioinformatics*, 90(1), 176-185.10.1002/prot.26205
18. Newman, J. A., Douangamath, A., Yadzani, S., Yosaatmadja, Y., Aimon, A., Brandão-Neto, J., Dunnett, L., Gorrie-Stone, T., Skyner, R., Fearon, D. & Schapira, M., (2021). Structure, mechanism and crystallographic fragment screening of the SARS-CoV-2 NSP13 helicase. *Nature communications*, 12(1), 1-11.10.1038/s41467-021-25166-6
19. Ma, Y., Wu, L., Shaw, N., Gao, Y., Wang, J., Sun, Y., … Rao, Z. (2015). Structural basis and functional analysis of the SARS coronavirus nsp14–nsp10 complex. Proceedings of the National Academy of Sciences, 112(30), 9436-9441.10.1073/pnas.1508686112
20. Pillon, M. C., Frazier, M. N., Dillard, L. B., Williams, J. G., Kocaman, S., Krahn,J. M., … Stanley, R. E. (2021). Cryo-EM structures of the SARS-CoV-2 endoribonuclease Nsp15 reveal insight into nuclease specificity and dynamics. *Nature Communications*, 12(1), 1-12.10.1038/s41467-020-20608-z
21. Nallusamy, S., Mannu, J., Ravikumar, C., Angamuthu, K., Nathan, B., Nachimuthu, K., Ramasamy, G., Muthurajan, R., Subbarayalu, M. & Neelakandan, K. (2021). Exploring phytochemicals of traditional medicinal plants exhibiting inhibitory activity against main protease, Spike glycoprotein, RNA-dependent RNA polymerase and non-structural proteins of SARS-CoV-2 through virtual screening. *Frontiers in Pharmacology*, 12, 1704.10.3389/fphar.2021.667704
22. Berman, H. M., Westbrook, J., Feng, Z., Gilliland, G., Bhat, T. N., Weissig, H., Shindyalov, I.N. & Bourne, P. E. (2000). The protein data bank. *Nucleic acids research*, 28(1), 235-242.10.1093/nar/28.1.235
23. Krafcikova, P., Silhan, J., Nencka, R., & Boura, E. (2020). Structural analysis of the SARS-CoV-2 methyltransferase complex involved in RNA cap creation bound to sinefungin. *Nature Communications*, 11(1), 1-7.10.1038/s41467-020-17495-9
24. Jin, Z., Du, X., Xu, Y., Deng, Y., Liu, M., Zhao, Y., Zhang, B., Li, X., Zhang, L., Peng, C. Duan, Y & Yang, H. (2020). Structure of Mpro from SARS-CoV-2 and discovery of its inhibitors. *Nature*, 582(7811), 289-293.10.1038/s41586-020-2223-y
25. Shin, D., Mukherjee, R., Grewe, D., Bojkova, D., Baek, K., Bhattacharya, A., … Dikic,I. (2020). Papain-like protease regulates SARS-CoV-2 viral spread and innate immunity. *Nature*, 587(7835), 657-662.10.1038/s41586-020-2601-5

26. Rizvi, S. M. D., Shakil, S., & Haneef, M. (2013). A simple click by click protocol to perform docking: AutoDock 4.2 made easy for non-bioinformaticians. EXCLI journal, 12, 831.
27. Seeliger, D., & de Groot, B. L. (2010). Ligand docking and binding site analysis with PyMOL and Autodock/Vina. *Journal of Computer-Aided Molecular Design*, 24(5), 417-422.10.1007/s10822-010-9352-6
28. Forli, S., Huey, R., Pique, M. E., Sanner, M. F., Goodsell, D. S., & Olson, A. J. (2016). Computational protein–ligand docking and virtual drug screening with the AutoDock suite. Nature protocols, *11*(5), 905–919. https://doi.org/10.1038/nprot.2016.051
29. Adeniji, S. E., Arthur, D. E., Abdullahi, M., & Haruna, A. (2020). Quantitative structure–activity relationship model, molecular docking simulation and computational design of some novel compounds against DNA gyrase receptor. Chemistry Africa, *3*, 391–408. https://doi.org/10.1007/s42250-020-00132-9
30. Cheng, F., Li, W., Zhou, Y., Shen, J., Wu, Z., Liu, G., Lee, P. W. & Tang, Y. (2012). admetSAR: a comprehensive source and free tool for assessment of chemical ADMET properties. *Journal of Chemical Information and Modeling 10*.1021/ci300367a
31. Ranjith, D., & Ravikumar, C. (2019). SwissADME predictions of pharmacokinetics and drug-likeness properties of small molecules present in Ipomoea mauritiana Jacq. Journal of Pharmacognosy and Phytochemistry, 8(5), 2063–2073.
32. Manzano, J. A., Pilapil, D. Y. H., Fernandez, R. A. T., Ching, J. K., Quimque, M. T. J., Notarte, K. I., & Macabeo, A. P. (2021). Repurposing Multi-Targeting Plant Natural Product Scaffolds in Silico against SARS-CoV-2 Non-Structural Proteins Implicated in Viral Pathogenesis. *Biological and Medicinal Chemistry.*10.26434/chemrxiv.14125433.v1
33. Nisha, C. M., Kumar, A., Nair, P., Gupta, N., Silakari, C., Tripathi, T., & Kumar, A. (2016). Molecular docking and in silico ADMET study reveals acylguanidine 7a as a potential inhibitor of β-secretase. *Advances in Bioinformatics*, 2016.
34. Wang, J., Kollman, P., Casw, D., & Wang, W. (2004). Antechamber, An Accessory Software Package For Molecular Mechanical Calculations. 222(1).
35. Sousa da Silva, A., &Vranken, W. (2012). ACPYPE - AnteChamberPYthon Parser interfacE. BMC Research Notes, 5(1). 10.1186/1756-0500-5-367.
36. Ash, S., Pyne, S., Misra, A., & De, S. (2010). Excited state intramolecular proton transfer in 3-hydroxy flavone and 5-hydroxy flavone: A DFT based comparative study. Journal of Molecular Modeling, 16(5), 831–839. 10.1007/s00894-009-0578-y.
37. Pettersen, E., Goddard, T., Couch, G., Meng, E., Ferrin, T., Huang, C., & Greenblatt, D. (2004). UCSF Chimera? A visualization system for exploratory research and analysis. Journal of Computational Chemistry, 25(13), 1605–1612. 10.1002/jcc.20084.
38. Berendsen, H., Drunen, R., & van der Spoel, D. (1995). GROMACS: A message-passing parallel molecular dynamics implementation. Computer Physics Communications, 91, 43–56.
39. Kutzner, C., Esztermann, A., Páll, S., Groot, B., Fechner, M., & Grubmüller, H. (2019). More bang for your buck: Improved use of GPU nodes for GROMACS 2018. Journal of Computational Chemistry, 40(27), 2418–2431. 10.1002/jcc.26011.

40. Lindorff-Larsen, K., Palmo, K., Piana, S., Klepeis, J., Shaw, D., Maragakis, P., &Dror, R. (2010). Improved side-chain torsion potentials for the Amber ff99SB protein force field: Improved Protein Side-Chain Potentials. Proteins: Structure, Function, and Bioinformatics, 78(8), 1950–1958. 10.1002/prot.22711.
41. Price, D., & Brooks, C. (2004). A modified TIP3P water potential for simulation with Ewald summation. The Journal of Chemical Physics, 121(20), 10096–10103. 10.1063/1.1808117.
42. Lemak, A., & Balabaev, N. (1994). On The Berendsen Thermostat. Molecular Simulation, 13(3), 177–187. 10.1080/08927029408021981.
43. Grubmüller, H., Windemuth, A., Heller, H., &Schulten, K. (1991). Generalized Verlet Algorithm for Efficient Molecular Dynamics Simulations with Long-range Interactions. Molecular Simulation, 6(1–3), 121–142. 10.1080/08927029108022142.
44. Essmann, U., Perera, L., Berkowitz, M., Pedersen, L., Darden, T., & Lee, H. (1995). A smooth particle mesh Ewald method. The Journal of Chemical Physics, 103(19), 8577–8593. 10.1063/1.470117.
45. Frazier, M., Krahn, J., Stanley, R., Wilson, I., Butay, K., Dillard, L., & Borgnia, M. (2022). Flipped over U: structural basis for dsRNA cleavage by the SARS-CoV-2 endoribonuclease. Nucleic Acids Research, 50(14), 8290–8301. 10.1093/nar/gkac589.
46. Bakan, A., Bahar, I., & Meireles, L. (2011). ProDy: Protein Dynamics Inferred from Theory and Experiments. Bioinformatics, 27(11), 1575–1577. 10.1093/bioinformatics/btr168.
47. Ismail, M. M., El-Zahabi, H. S., Ibrahim, R. S., & Mehany, A. B. (2020). Design and synthesis of novel tranilast analogs: Docking, antiproliferative evaluation and in-silico screening of TGFβR1 inhibitors. Bioorganic Chemistry, *105*, 104368. https://doi.org/10.1016/j.bioorg.2020.104368
48. Pandey, P., Singh, D., Hasanain, M., Ashraf, R., Maheshwari, M., Choyal, K., … Sarkar,J. (2019). 7-hydroxyfrullanolide, isolated from Sphaeranthus indicus, inhibits colorectal cancer cell growth by p53-dependent and-independent mechanism. *Carcinogenesis*, 40(6), 791-804.10.1093/carcin/bgy176
49. Ambavade, S. D., Mhetre, N. A., Tate, V. D., & Bodhankar, S. L. (2006). Pharmacological evaluation of the extracts of Sphaeranthus indicus flowers on anxiolytic activity in mice. *Indian Journal of Pharmacology*, 38(4), 254.10.4103/0253-7613.27021
50. Machado, R. R., Valente Júnior, W., Lesche, B., Coimbra, E. S., Souza, N. B. D., Abramo, C., Soares, G.L.G. & Kaplan, M. A. C. (2012). Essential oil from leaves of Lantana camara: a potential source of medicine against leishmaniasis. *Revista Brasileira de Farmacognosia*, 22, 1011-1017.10.1590/S0102-695X2012005000057
51. Kalita, S., Kumar, G., Karthik, L., & Rao, K. V. B. (2012). A Review on Medicinal Properties of Lantana camara Linn. Research Journal of Pharmacy and Technology, 5(6), 711–715.
52. Tungmunnithum, D., Pinthong, D., &Hano, C. (2018). Flavonoids from Nelumbo nucifera Gaertn., a medicinal plant: Uses in traditional medicine, phytochemistry and pharmacological activities. *Medicines*, 5(4), 127.10.3390/medicines5040127
53. Gorlenko, C., Kiselev, H., Budanova, E., Zamyatnin, A., & Ikryannikova, L. (2020). Plant Secondary Metabolites in the Battle of Drugs and Drug-Resistant Bacteria: New Heroes or Worse Clones of Antibiotics?.*Antibiotics*, 9(4), 170. 10.3390/antibiotics9040170.

54. Humphrey, W., Schulten, S., &Dalke, A. (1996). VMD: visual molecular dynamics. 14(1), 33–38. 10.1016/0263–7855(96)00018 – 5.
55. Jakalian, A., Jack, D., & Bayly, C. (2002). Fast, efficient generation of high-quality atomic charges. AM1-BCC model: II. Parameterization and validation. Journal of Computational Chemistry, 23(16), 1623–1641. 10.1002/jcc.10128.

Figures

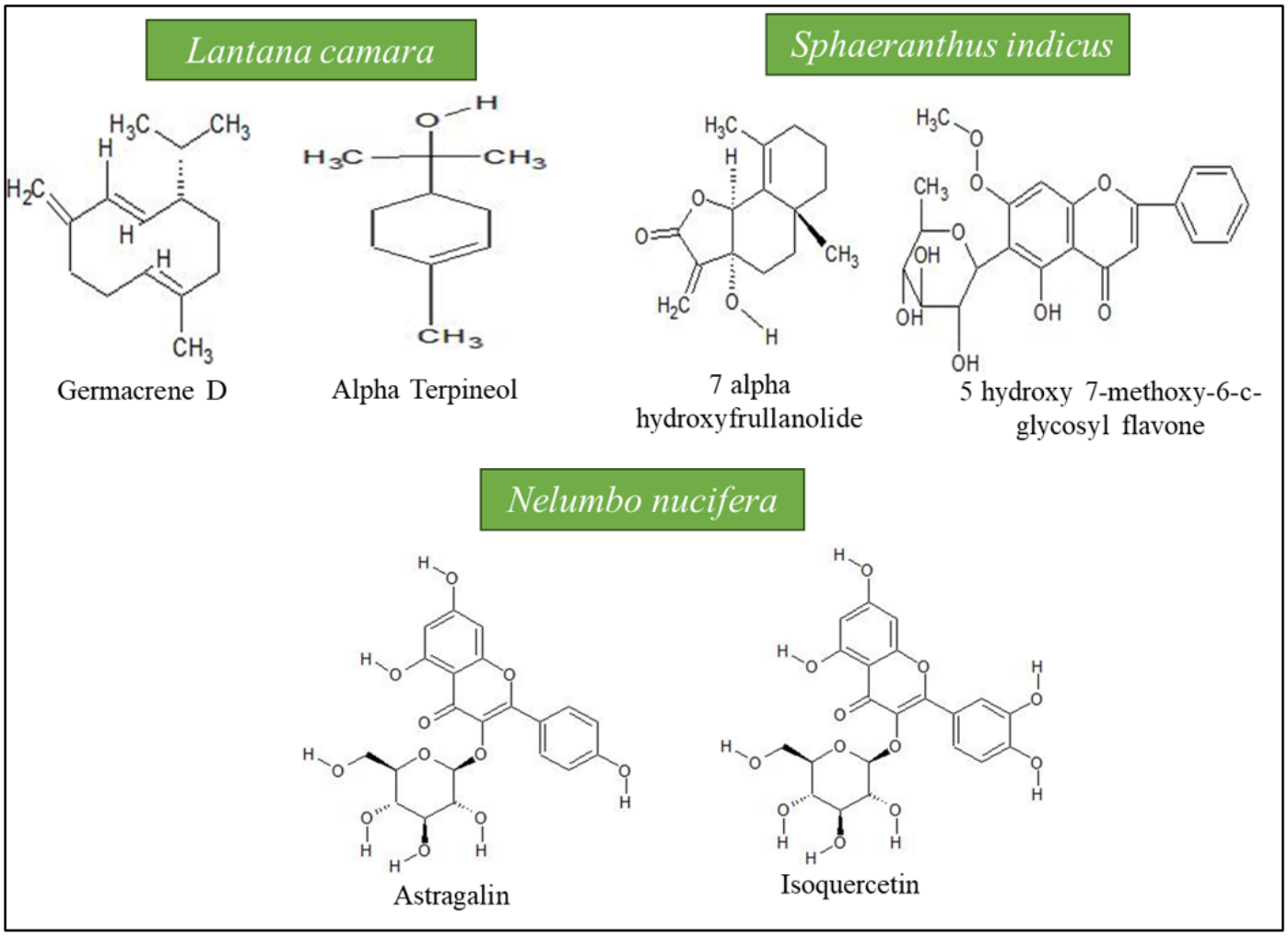

Figure 1

Phytocompounds of selected plants

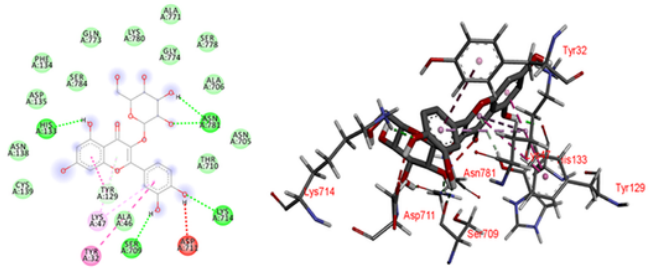

Figure 2a.

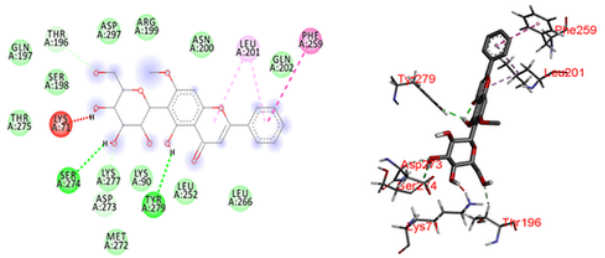

Figure 2c.

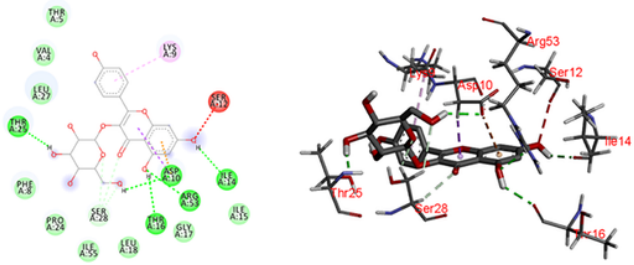

Figure 2b.

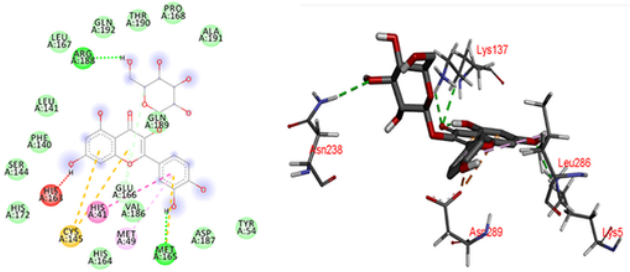

Figure 2d.

Figure 2

a. 2D and 3D interactions of NSP12 and Isoquercetin with binding energy -8.2 kcal/mol

b. 2D and 3D interactions of NSP14 and Astragalin with binding energy -8.1 kcal/mol

c. 2D and 3D interactions of NSP15 and 5-hydroxy-7-methoxy -6-c-glycosy flavone with binding energy -9.3 kcal/mol

d. 2D and 3D interactions of NSP5 and Isoquercetin with binding energy -8.2 kcal/mol

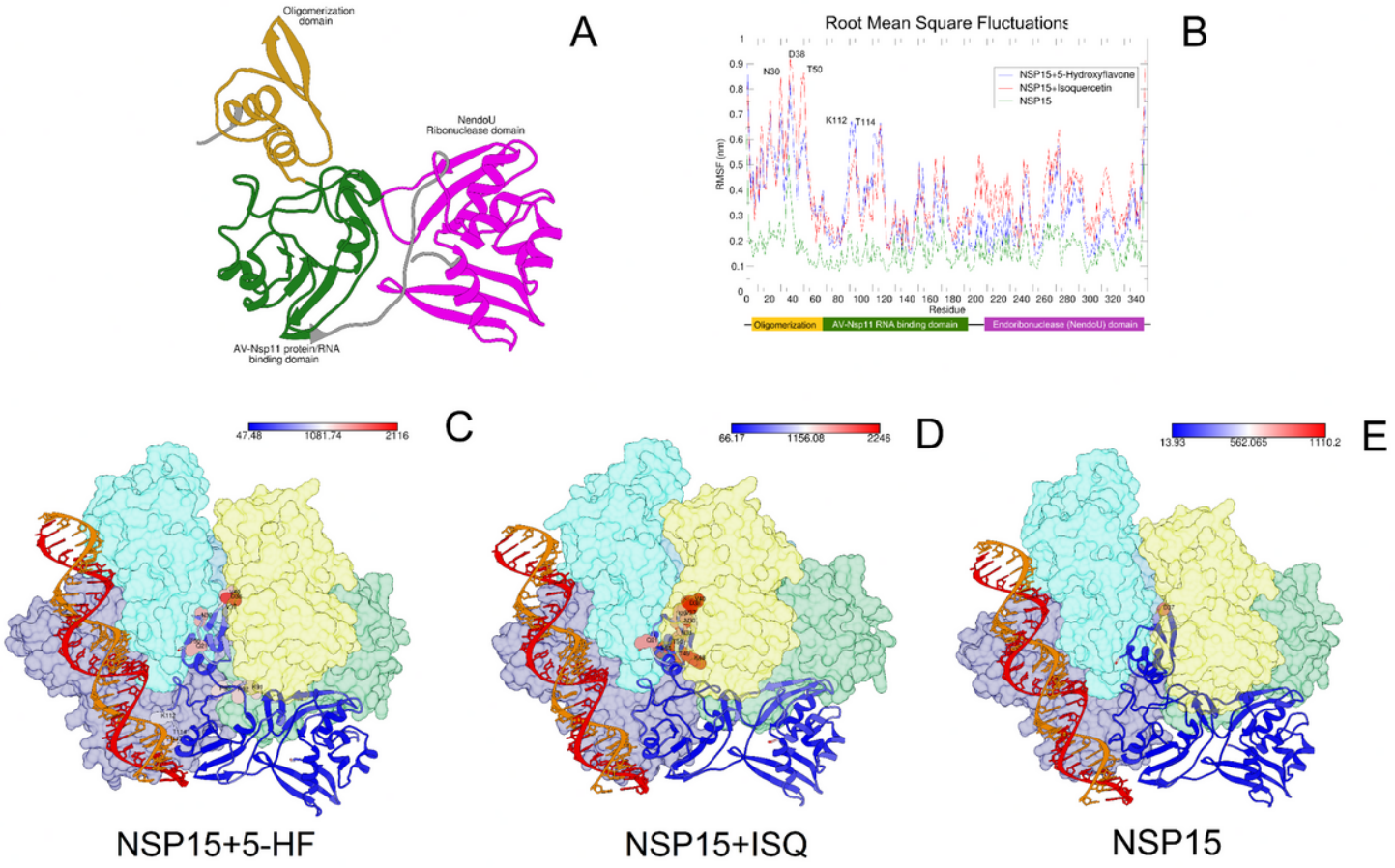

Figure 3

Fig. 5. A: Domain architecture of SARS-CoV2 NSP15 protein. The domain architecture is based on the PROSITE annotation of NSP15 domain boundaries (Sigrist et al. 2012, Sigrist et al. 2005). B: RMSF plot of NSP15 residues from the simulation trajectories. Calculations were performed on all the atoms of NSP15. Domain boundaries of NSP15 are represented as bars below the y-axis. Residues having highest fluctuations are labelled. C,D,E: Representation of RMSF as B-factors from the simulations of 5-HF(C), ISQ (D) bound to NSP15 and apo-state simulations of NSP15 (E). The structure of NSP15 with RMSF represented as B-factors was superimposed to the hexameric cryo-EM structure of SARS-CoV2 NSP15, bound to double-stranded RNA (Frazier et al. 2022; PDB: 7TJ2). Superimposition and visualization was performed using UCSF Chimera program (Petterson et al. 2004).

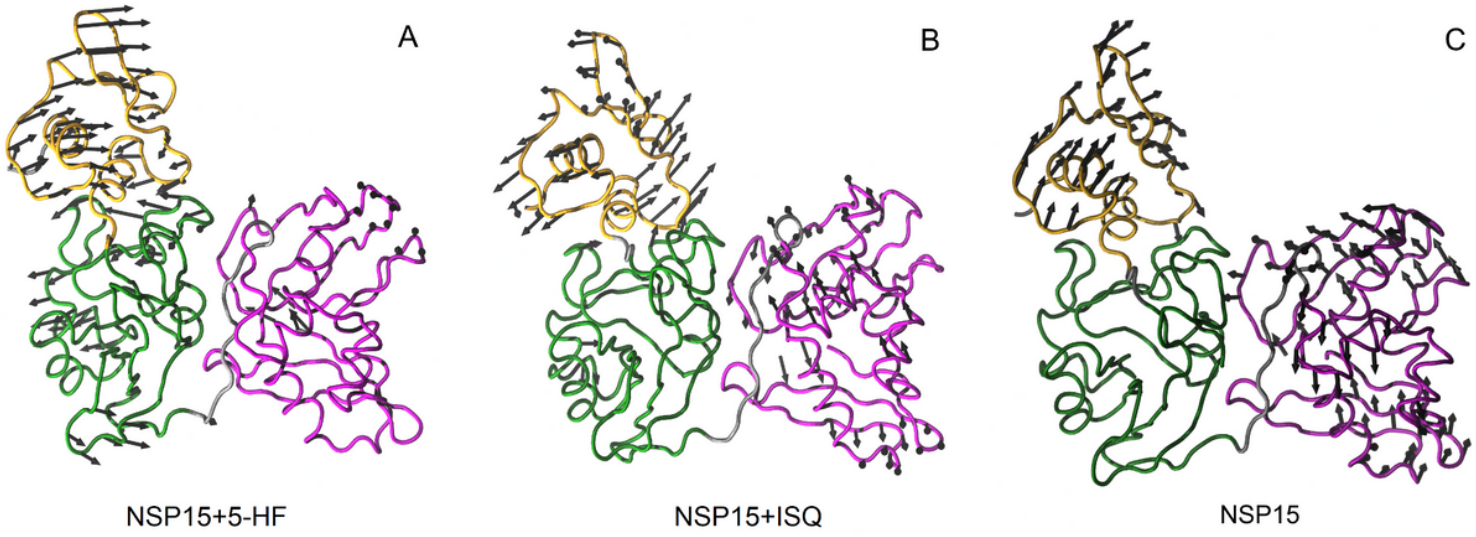

Figure 4

Fig. 6. Representation of the essential dynamics of first principal components from the trajectory ensembles of 5-HF (A) and ISQ (B) bound to NSP15, and NSP15 in the apo-state. The first principal components correspond to 22%, 43% and 22% of the trajectories respectively. Oligomerization, Nsp11 RNA-binding and NendoU ribonuclease domains are represented as Yellow, Green and Magenta tubes respectively. Direction of dynamics of the residues with fluctuations >2Å are represented as black arrows. Dynamics was visualized using the VMD program.

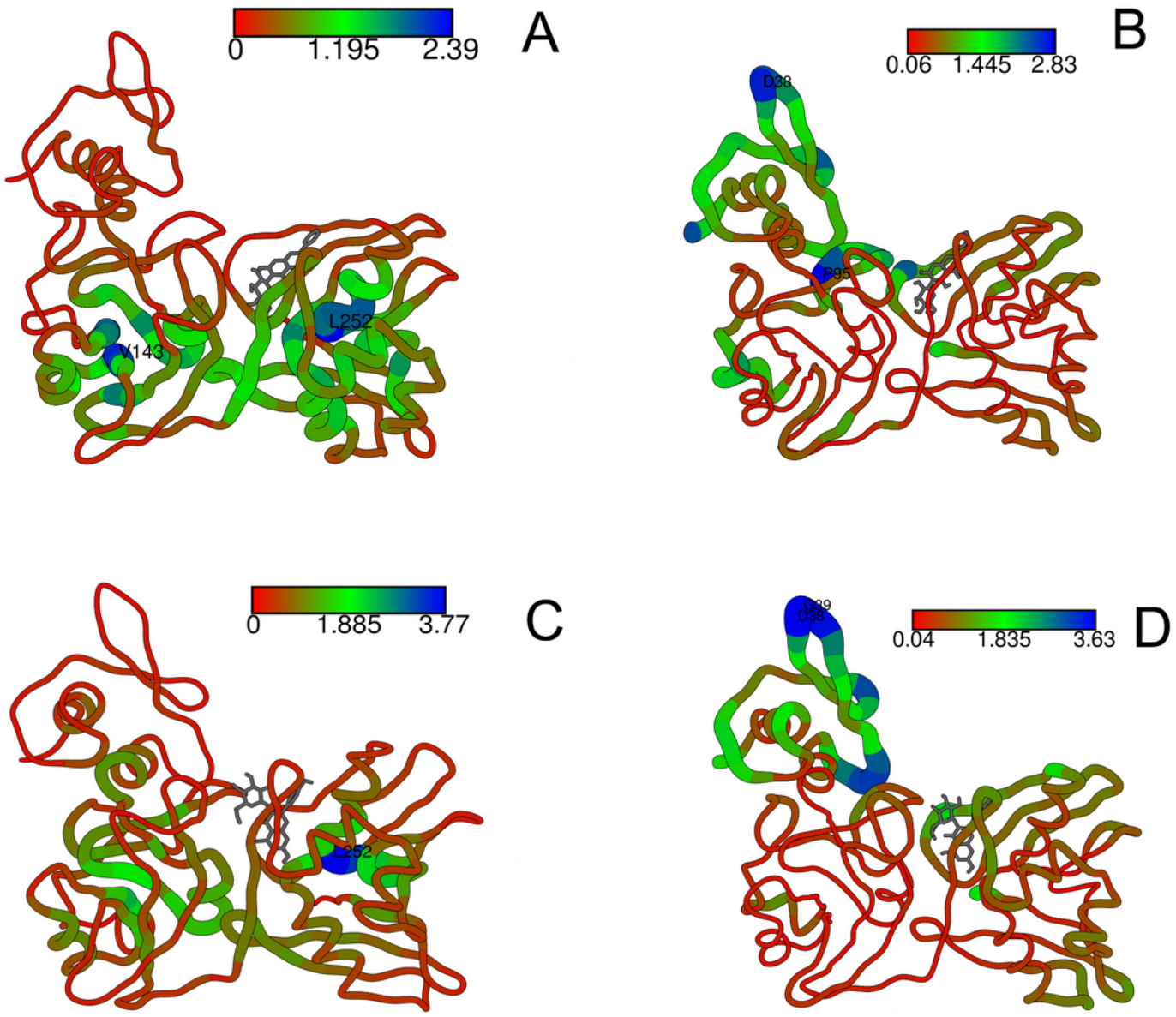

Figure 5

Fig. 7. Projection of sensitivity and effectiveness profiles of NSP15 residues over the NSP15 structure. Calculations were performed from the NSP15 simulations with different ligands. A: Sensitivity profile of NSP15 residues in presence of 5-HF. B: Effectiveness profile of NSP15 in presence of 5-HF. C: Sensitivity profile of NSP15 residues in presence of ISQ. D: Effectiveness profile of NSP15 residues in presence of ISQ. Residues with highest sensitivity/effectiveness are represented in blue, residues with lowest sensitivity/effectiveness are reprsented in red. The thickness of the tube corresponds to the sensetivity/effectiveness propensity of the given residue. Calculations were performed using the ProDy program (Bakan et al. 2011, Dutta et al. 2015), visualization performed using UCSF Chimera program (Pettersen et al. 2014).

Supplementary Files

This is a list of supplementary files associated with this preprint. Click to download.

- GA.png
- Supplementary.docx